JACS Au
AN OPEN ACCESS JOURNAL OF THE AMERICAN CHEMICAL SOCIETY

pubs.acs.org/jacsau

Article

Antisymmetric Spin Exchange in a μ-1,2-Peroxodicopper(II) Complex with an Orthogonal Cu–O–O–Cu Arrangement and S = 1 Spin Ground State Characterized by THz-EPR

Thomas Lohmiller,[#] Can-Jerome Spyra,[#] Sebastian Dechert, Serhiy Demeshko, Eckhard Bill, Alexander Schnegg,* and Franc Meyer*

Cite This: *JACS Au* 2022, 2, 1134–1143

Read Online

ACCESS | Metrics & More | Article Recommendations | Supporting Information

ABSTRACT: A unique type of Cu_2/O_2 adduct with orthogonal (close to 90°) Cu–O–O–Cu arrangement has been proposed for initial stages of O_2 binding at biological type III dicopper sites, and targeted ligand design has now allowed us to emulate such an adduct in a pyrazolate-based μ-η^1:η^1-peroxodicopper(II) complex (**2**) with Cu–O–O–Cu torsion φ of 87°, coined $^{\perp}$**P** intermediate. Full characterization of **2**, including X-ray diffraction (d_{O-O} = 1.452 Å) and Raman spectroscopy ($\tilde{\nu}_{O-O}$ = 807 cm^{-1}), completes a series of closely related Cu_2/O_2 intermediates featuring μ-η^1:η^1-peroxodicopper(II) cores with φ ranging from 55° (**A**, *cis*-peroxo ^{C}**P**; Brinkmeier, A. *et al., J. Am. Chem. Soc.* **2021**, *143*, 10361) via 87° (**2**, $^{\perp}$**P** type) up to 104° (**B**, approaching *trans*-peroxo ^{T}**P**; Kindermann, N. *et al., Angew. Chem., Int. Ed.* **2015**, *54*, 1738). SQUID magnetometry revealed ferromagnetic interaction of the Cu^{II} ions and a triplet (S_t = 1) ground state in **2**. Frequency-domain THz-EPR has been employed to quantitatively investigate the spin systems of **2** and **B**. Magnetic transitions within the triplet ground states confirmed their substantial zero-field splittings (ZFS) suggested by magnetometry. Formally forbidden triplet-to-singlet transitions at 56 (**2**) and 157 cm^{-1} (**B**), which are in agreement with the exchange coupling strengths J_{iso} inferred from SQUID data, are reported for the first time for coupled dicopper(II) complexes. Rigorous analysis by spin-Hamiltonian-based simulations attributed the corresponding nonzero transition probabilities and the ZFS to substantial antisymmetric (Dzyaloshinskii–Moriya) exchange ***d*** and provided robust values and orientations for the ***d***, ***J***, and ***g*** tensors. These interactions can be correlated with the Cu–O–O–Cu geometries, revealing a linear increase of J_{iso} with the Cu–O–O–Cu torsion and a strong linear decrease with the Cu–O–O angle. Relevance of the $^{\perp}$**P** intermediate for O_2 activation at type III dicopper sites and a potential role of antisymmetric exchange in the concomitant intersystem crossing are proposed.

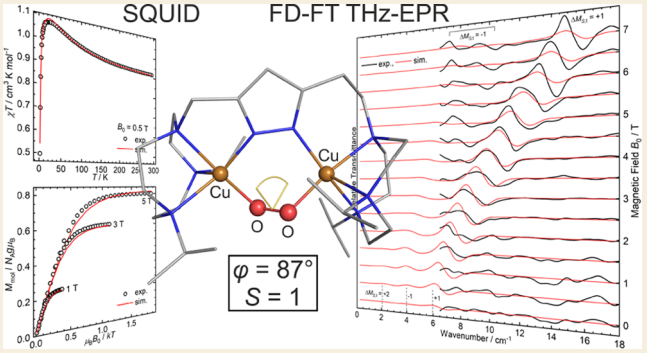

KEYWORDS: *dioxygen activation, copper complexes, THz-EPR spectroscopy, ferromagnetic coupling, zero-field splitting, Dzyaloshinskii–Moriya interaction, magnetostructural correlation*

INTRODUCTION

Binding and activation of dioxygen at type III copper metalloproteins, such as hemocyanine, catechol oxidase, and tyrosinase, is a textbook case in bioinorganic chemistry and has been intensively investigated.[1−3] Significant progress on the understanding of biological dicopper/dioxygen chemistry has been achieved through the combined use of computational and advanced spectroscopic methods as well as the development of synthetic analogues.[4−6] Several types of Cu_2/O_2 intermediates have been identified upon exposure of copper(I) model complexes to dioxygen (Scheme 1, top). *trans*-μ-η^1:η^1- (^{T}**P**) and μ-η^2:η^2-peroxodicopper(II) (^{S}**P**) complexes have been quite well studied,[7−9] and they are generally found to have a strongly stabilized total spin S_t = 0 ground state due to antiferromagnetic coupling between the two Cu^{II} ions. Examples of isolated Cu_2/O_2 adducts with a *cis*-μ-η^1:η^1 peroxo motif (^{C}**P**) are relatively scarce, and structural characterization has been achieved only recently.[10−12] While the ^{S}**P** core represents the key intermediate identified in oxygenated type III copper proteins, species with a μ-η^1:η^1-peroxo unit have been proposed along the trajectory of O_2 binding/release at these biological dicopper sites, based on computational work by Solomon and co-workers.[13−15] In this scenario, binding of

Received: February 28, 2022
Revised: April 8, 2022
Accepted: April 11, 2022
Published: May 6, 2022

https://doi.org/10.1021/jacsau.2c00139
JACS Au 2022, 2, 1134–1143

Scheme 1. Structurally Characterized Cu_2/O_2 Motifs (Top) and the Mechanism for O_2 Binding at Type III Dicopper Sites Involving a $^{\perp}$P Arrangement on the Way to the ^{S}P Intermediate (Bottom)

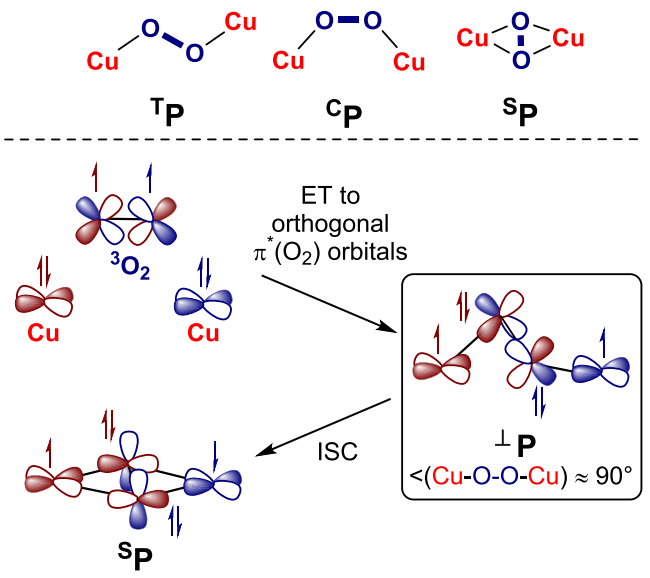

triplet dioxygen initially proceeds via simultaneous electron transfer from the two Cu^{I} ions to the two orthogonal dioxygen π^* orbitals, whereby $^3O_2$ is reduced to $^1O_2^{2-}$. Delocalization of the unpaired spins to the copper(II) ions results in sizeable ferromagnetic coupling (Scheme 1). The triplet (S_t = 1) ground state prevails in a μ-η^1:η^1-peroxodicopper(II) arrangement with Cu−O−O−Cu torsion angle close to 90° (which we now coin $^{\perp}$**P**, distinct from ^{T}**P** and ^{C}**P** species with limiting Cu−O−O−Cu torsion angles of around 180 or 0°, respectively). This initial binding mode then progresses to the planar Cu_2O_2 core (^{S}**P**) while establishing a superexchange pathway and enabling the triplet-to-singlet intersystem crossing (ISC) and hence the formation of the experimentally observed S_t = 0 ground state for type III copper proteins.[13−15]

By employing a compartmental pyrazolate/tacn (tacn = 1,4,7-triazacyclononane) hybrid ligand $[L^{1,1}]^-$, we could isolate and structurally characterize μ-1,2-peroxodicopper(II) complex **A** (Figure 1) in which the dinucleating ligand scaffold enforces a *cis*-μ-η^1:η^1-peroxo (^{C}**P** type) binding mode, showing a Cu−O−O−Cu dihedral angle φ of around 55°.[10,11] Modification of the ligand scaffold by elongating the linker units between the tacn side arms and the central pyrazolate bridge ($[L^{2,2}]^-$) induces a shorter Cu···Cu distance and consequently a tilting of the peroxo unit within the bimetallic pocket (**B**; Figure 1).[16] This results in a Cu−O−O−Cu dihedral angle even beyond 90° in **B**, viz. φ = 104°, and dramatically different magnetic properties: while **A** features an S_t = 0 ground state (though antiferromagnetic coupling is relatively weak, J_{iso} = −56 cm^{-1}; $\hat{H} = -2J_{iso}\,\hat{S}_1\,\hat{S}_2$), **B** shows significant ferromagnetic coupling (S_t = 1, J_{iso} = +72 cm^{-1}). Complex **B** is the first, and so far the only, peroxodicopper(II) complex with an S_t = 1 ground state that can be viewed as a model of the $^{\perp}$**P** situation shown in Scheme 1. Interestingly, multifield magnetization measurements for **B** suggested an unexpected large zero-field splitting (ZFS) $|D_t| \approx 3$ cm^{-1} of the total spin S_t =1 ground state. This is quite unusual for a spin pair with local spin doublets, S_i = 1/2.[16] The magnetic data were well simulated by including antisymmetric exchange in the spin-Hamiltonian, but the

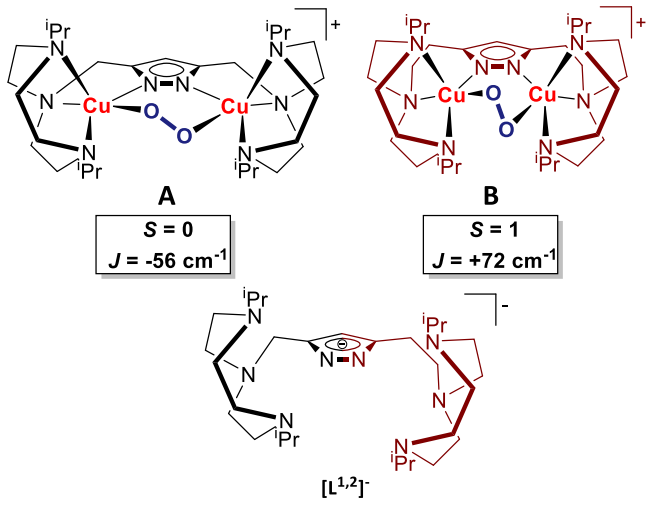

Figure 1. Previously reported peroxodicopper(II) complexes A and B based on the pyrazolate/tacn ligands $[L^{1,1}]^-$ and $[L^{2,2}]^-$, respectively, and the nonsymmetric ligand $[L^{1,2}]^-$ presented in this work.

magnitude of the ZFS so far prevented its direct determination via spectroscopic detection of transitions within the triplet ground-state multiplet. Antisymmetric or Dzyaloshinskii−Moriya (DM) exchange results from the concerted action of single-ion spin−orbit coupling (SOC) and exchange coupling between ground and excited states of different paramagnetic ions in a noninversion-symmetric environment.[17−19]

Complexes **A** and **B** demonstrate the impact of targeted ligand modifications on the resulting structural and electronic properties of the Cu_2/O_2 adducts. The aim of the present study was threefold: (i) adjusting the Cu−O−O−Cu torsion to closely match the orthogonal arrangement with φ = 90° in an exact $^{\perp}$**P** model; (ii) examining the effect of variable torsion angles φ on spin-spin coupling in the μ-η^1:η^1-peroxodicopper(II) core; and (iii) spectroscopically measuring the ZFS of the S_t = 1 ground state in **B** and the new $^{\perp}$**P** model. To this end, we have now employed the hybrid ligand scaffold $[L^{1,2}]^-$ that combines structural components of ligands $[L^{1,1}]^-$ and $[L^{2,2}]^-$ present in **A** and **B**, viz. one short (CH_2) and one longer (CH_2CH_2) linker between the tacn side arms and the central pyrazolate bridge (Figure 1). Furthermore, we have used a combination of SQUID magnetometry and frequency-domain Fourier-transform (FD-FT) THz-EPR spectroscopy[20,21] as a novel method for directly detecting the respective spin-state transitions and to yield refined insights into the electronic structure of these unique ferromagnetically coupled Cu_2/O_2 adducts.

RESULTS AND DISCUSSION

The nonsymmetrical ligand scaffold $[L^{1,2}]^-$ was synthesized according to previously reported multistep protocols[22,23] with slight modifications, which are described in detail in Section 2 of the Supporting Information (SI). For the synthesis of dicopper(I) complex **1**, $HL^{1,2}$ was deprotonated with potassium *tert*-butoxide, and the resulting ligand $[L^{1,2}]^-$ was reacted with two equivalents of $[Cu(MeCN)_4]ClO_4$. Subsequent counter ion exchange with $NaBPh_4$ led to the isolation of the dicopper(I) complex $[L^{1,2}Cu_2]BPh_4$ (**1**). The structure of **1** was determined by X-ray diffraction of single crystals grown from acetone/diethyl ether solutions, containing two independent molecules of **1** per asymmetric unit; the

https://doi.org/10.1021/jacsau.2c00139
JACS Au 2022, 2, 1134−1143

molecular structure of its cation is depicted in Figure 2. Both Cu^{I} ions are found in distorted tetrahedral coordination

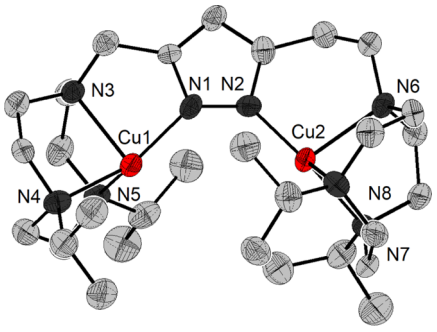

Figure 2. Molecular structure of the cation of dicopper(I) complex **1**. Thermal displacement ellipsoids are given at 50% probability. Hydrogen atoms, solvent molecules, and counter ions are omitted for clarity.

environment (τ_4 = 0.64 (Cu1), 0.60 (Cu2)[24]) within the $\{N_4\}$ binding pockets of the pyrazolate/tacn framework. The Cu···Cu distance is 4.081 Å and 4.060 Å for the two crystallographically independent molecules, which is in between the values previously reported for dicopper(I) complexes $[L^{1,1}Cu_2]BPh_4$ (4.153 Å) and $[L^{2,2}Cu_2]BPh_4$ (3.968 Å), demonstrating the tunability of the metal···metal separation by targeted ligand design.[11,16] Diamagnetic complex **1** was also characterized by NMR spectroscopy (SI, Section 3.1).

Colorless solutions of complex **1** in MeCN or EtCN react readily with molecular dioxygen, accompanied by an intense purple colorization (Figure S9), indicating the formation of the corresponding peroxo complex $[L^{1,2}Cu_2(O_2)]^+$ (cation of **2**). Following the reaction by UV/vis absorption spectroscopy (Figure S8) shows the emergence of a dominant peak at 520 nm ($\varepsilon \approx 5500\ M^{-1}\ cm^{-1}$) with shoulders at 617 nm ($\varepsilon \approx 3300\ M^{-1}\ cm^{-1}$) and 790 nm ($\varepsilon \approx 1500\ M^{-1}\ cm^{-1}$), as well as a less pronounced shoulder at higher energy around 430 nm ($\varepsilon \approx 2000\ M^{-1}\ cm^{-1}$). These distinct features are characteristic of μ-η^1:η^1-peroxodicopper(II) complexes, mostly due to $O_2^{2-} \rightarrow Cu^{II}$ charge transfer transitions.[5,6] In particular, the spectrum of **2** is very similar to that of complex **B** (Figure 3), whereas complex **A** reveals a distinct maximum at 648 nm that was

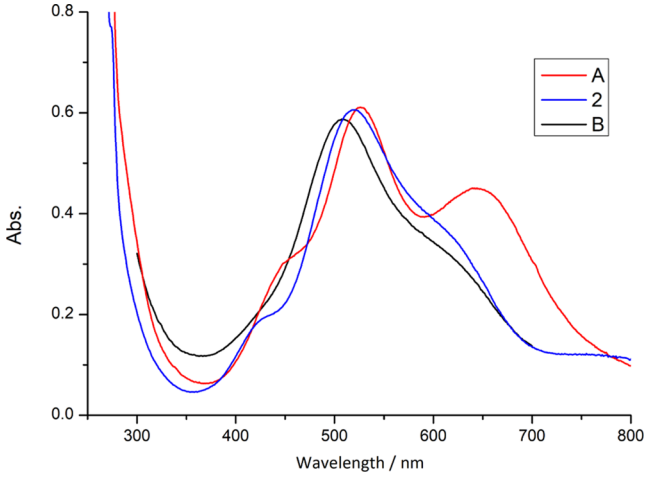

Figure 3. Electronic absorption spectra of peroxodicopper(II) complexes **A**, **2**, and **B** in MeCN at −40 °C.

recently attributed by TD-DFT calculations to excitations within the π-manifold on the $Cu-O_2-Cu$ core.[11,12] Comparison of the three spectra indicates subtle electronic differences within this series of peroxodicopper(II) complexes based on the dinucleating pyrazolate/tacn ligands.

The resonance Raman spectrum of peroxo complex **2** (λ_{ex} = 633 nm; Figure 4) shows an intense feature at 807 cm^{-1} that

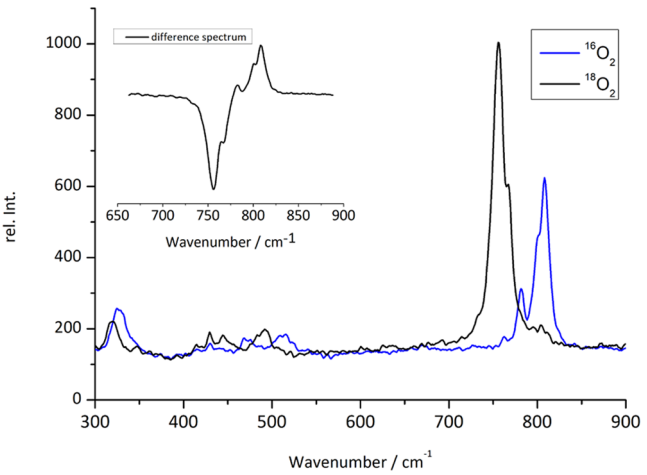

Figure 4. Resonance Raman spectra of crystalline complex **2** at room temperature (λ_{ex} = 633 nm); the inset shows the difference spectrum.

shifts to 757 cm^{-1} upon $^{18}O_2$ labeling ($\Delta(^{16}O_2-^{18}O_2)$ = 50 cm^{-1}; $\tilde{\nu}(^{16}O-^{16}O)/\tilde{\nu}(^{18}O-^{18}O)$ = 1.066, calculated 1.060 for an isolated harmonic O−O oscillator) and is therefore assigned to the O−O stretch. The value is very similar to the O−O stretching frequency of **B** (803 cm^{-1}, $\Delta(^{16}O_2-^{18}O_2)$ = 54 cm^{-1}), and also quite similar to the one of **A** (793 cm^{-1}, $\Delta(^{16}O_2-^{18}O_2)$ = 41 cm^{-1}). In MeCN solution, samples of **2** prepared from natural abundance O_2 show further peaks at 764, 783, and 800 cm^{-1} (Figure S10). This phenomenon was already observed for $[L^{1,1}Cu_2O_2]^+$ and to a lesser extent for $[L^{2,2}Cu_2O_2]^+$,[11,16] and it was tentatively attributed to Fermi resonance. Another possible explanation for **2** is the formation of isomers in solution due to the decreased symmetry of the nonsymmetric ligand scaffold $[L^{1,2}]^-$ combined with the shallow potential energy surface associated with changes of the Cu−O−O−Cu torsion.[11] A further isotope-sensitive band for solid **2** at 515 cm^{-1} ($\Delta(^{16}O_2-^{18}O_2)$ = 23 cm^{-1}) is assigned to the Cu−O stretch, and again this is very similar to the value observed for **B** (512 cm^{-1}, $\Delta(^{16}O_2-^{18}O_2)$ = 22 cm^{-1}). Overall, the electronic absorption and Raman spectra indicate close similarity of the peroxodicopper(II) cores of **2** and **B**.

By slow vapor diffusion of diethyl ether into an acetone solution of $[L^{1,2}Cu_2O_2]BPh_4$ (**2**) at −26 °C, single crystals suitable for X-ray analysis were obtained. These crystals are stable for months at room temperature under exclusion of water. As for the previously reported pyrazolate/tacn peroxodicopper(II) complexes **A** and **B**, the molecular structure of **2** shows a μ-η^1:η^1-peroxo unit within the bimetallic pocket (Figure 5). The O−O bond length (1.452 Å) and the Cu···Cu distance (3.696 Å) in **2** are right in between those of **A** (1.441, 3.741 Å) and **B** (1.460, 3.677 Å); Table 1 lists selected metric parameters for the three complexes. The coordination geometries of both copper ions in **2** differ slightly because of the nonsymmetric nature of the ligand scaffold: Cu1, hosted in the compartment with the shorter, methylene

https://doi.org/10.1021/jacsau.2c00139
JACS Au 2022, 2, 1134−1143

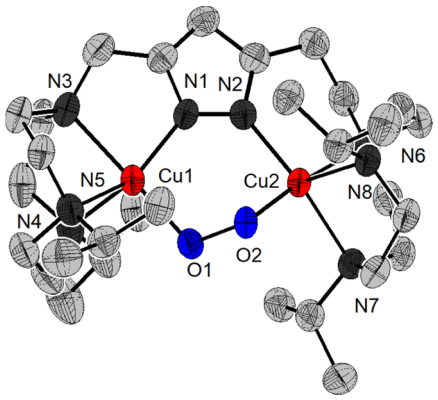

Figure 5. Molecular structure of the cation of **2**. Thermal displacement ellipsoids are given at 50% probability. Hydrogen atoms, solvent molecules, and counter ions are omitted for clarity.

spaced side arm, features a strongly distorted trigonal bipyramidal geometry (τ_5 = 0.55), while Cu2 in the compartment with the longer, ethylene spaced side arm exhibits a slightly distorted square pyramidal geometry (τ_5 = 0.20). These geometries appear to be imposed by the specific binding pockets as they are essentially the same as in the respective symmetric congeners **A** (τ_5 = 0.60) and **B** (τ_5 = 0.20) with two short or long side arms, respectively.[11,16]

Most interestingly, the Cu−O−O−Cu torsion angle φ in solid **2** is 87°, very close to the sought-after orthogonal arrangement for an ideal $^{\perp}$**P** intermediate. Therefore, targeted ligand design has now allowed for spanning the range of dihedral Cu−O−O−Cu angles from 55° (in **A** with ligand $[L^{1,1}]^-$) via 87° (in **2** with ligand $[L^{1,2}]^-$) to 104 ° (in **B** with ligand $[L^{2,2}]^-$), with the Cu^{II} ions being nested in very similar $\{N_4\}$ binding sites for the entire series. Figure 6 illustrates the different Cu···Cu separations enforced by the ligand scaffold, the different twisting of the peroxo unit within the bimetallic cleft, and the resulting changes in the Cu−O−O−Cu dihedral angle φ.

The clean isolation of **2** further allowed us to examine its magnetic properties via SQUID magnetometry; it should be noted that experimental variable temperature magnetic data for peroxodicopper(II) intermediates are still scarce in the literature.[10,12,16,25] Magnetic susceptibilities shown in Figure 7b were recorded in the temperature range of 2−295 K at 0.5 T and revealed ferromagnetic spin coupling and an S_t = 1 ground state, reflected by a distinct maximum of $\chi_m T$ between 20 and 30 K. Further, $\chi_m T$ rapidly decreases below 20 K, and multifield magnetization measurements at 1, 3, and 5 T (Figure 7c) revealed significant nesting of the $M(\mu_B B/kT)$ curves, suggesting sizable zero-field splitting (ZFS).

This rather unusual phenomenon for a system with two local spin doublets (S_i = 1/2), which cannot contribute single-ion ZFS, was also observed for **B**.[16] In the spin-Hamiltonian formalism for two spin-coupled Cu(II) ions, ZFS of the total spin triplet state can only be caused by symmetric or

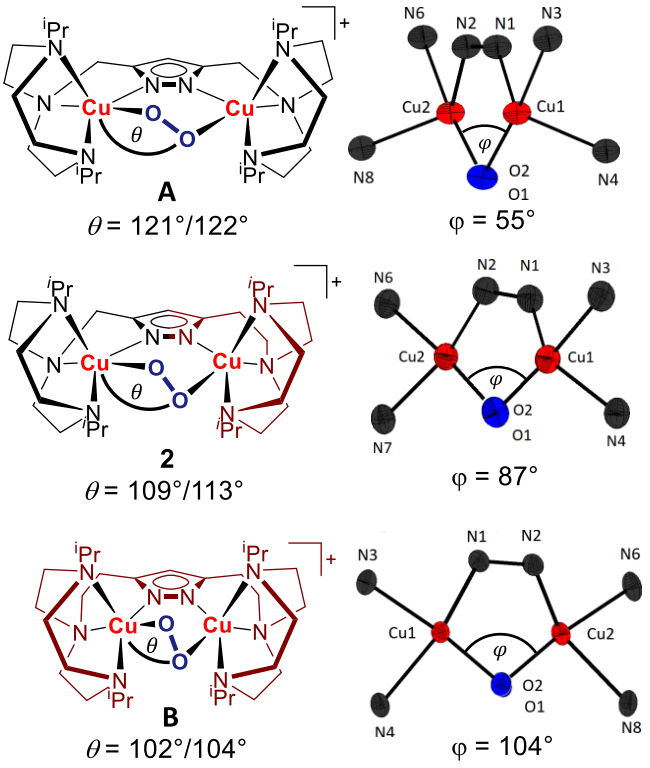

Figure 6. Series of peroxodicopper(II) complexes **A**,[11] **2**, and **B**[16] with Cu−O−O angles θ (left) and their core structures. The Cu−O−O−Cu torsion angle φ is visualized by looking along the O1−O2 bond of the core structures determined by X-ray diffraction (right).

antisymmetric anisotropic contributions to the exchange interaction. Since symmetric anisotropic coupling in peroxo complexes with long Cu···Cu distances and moderately strong isotropic exchange is not expected to play a crucial role, antisymmetric spin coupling was invoked to explain the unusual ZFS for **B**.[16]

The interaction of two Si = 1/2 spins is described by the following contributions to the spin-Hamiltonian: the isotropic Heisenberg−Dirac−van−Vleck exchange ($\hat{H}_{HDvV}$), the symmetric anisotropic exchange ($\hat{H}_{ani}$) and the antisymmetric Dzyaloshinskii−Moriya ($\hat{H}_{DM}$) term. The dipolar interaction was not considered explicitly as, based on the point-dipole model, its contribution to the magnetic anisotropy, or ZFS, is negligible. In the presence of an external magnetic field, a Zeeman term ($\hat{H}_{Zeeman}$) is added to the Hamiltonian

$$\begin{aligned}\hat{H} &= \hat{H}_{HDvV} + \hat{H}_{ani} + \hat{H}_{DM} + \hat{H}_{Zeeman} \\ &= -2J_{iso}\hat{\mathbf{S}}_1\hat{\mathbf{S}}_2 - 2\hat{\mathbf{S}}_1\mathbf{J}_{ani}\hat{\mathbf{S}}_2 + \mathbf{d}(\hat{\mathbf{S}}_1 \times \hat{\mathbf{S}}_2) + \mu_B\mathbf{B}_0(\mathbf{g}_1\hat{\mathbf{S}}_1 \\ &\quad + \mathbf{g}_2\hat{\mathbf{S}}_2) \end{aligned} \quad (1)$$

Analysis of magnetometry data is very powerful for a macroscopic assignment of the spin coupling scenario in multinuclear complexes. However, a robust and unambiguous

Table 1. Selected Structural Parameters of Pyrazolate/tacn-Based Peroxodicopper(II) Complexes A,[11] 2, and B[16]

	d(O−O) [Å]	φ(Cu1−O_2−Cu2) [deg]	θ(Cu1,2−O_2) [deg]	τ_5(Cu1,2)
A	1.441	55	121, 122	0.60, 0.63
2	1.452	87	109, 113	0.55, 0.20
B	1.460	104	102, 104	0.20, 0.20

https://doi.org/10.1021/jacsau.2c00139
JACS Au 2022, 2, 1134−1143

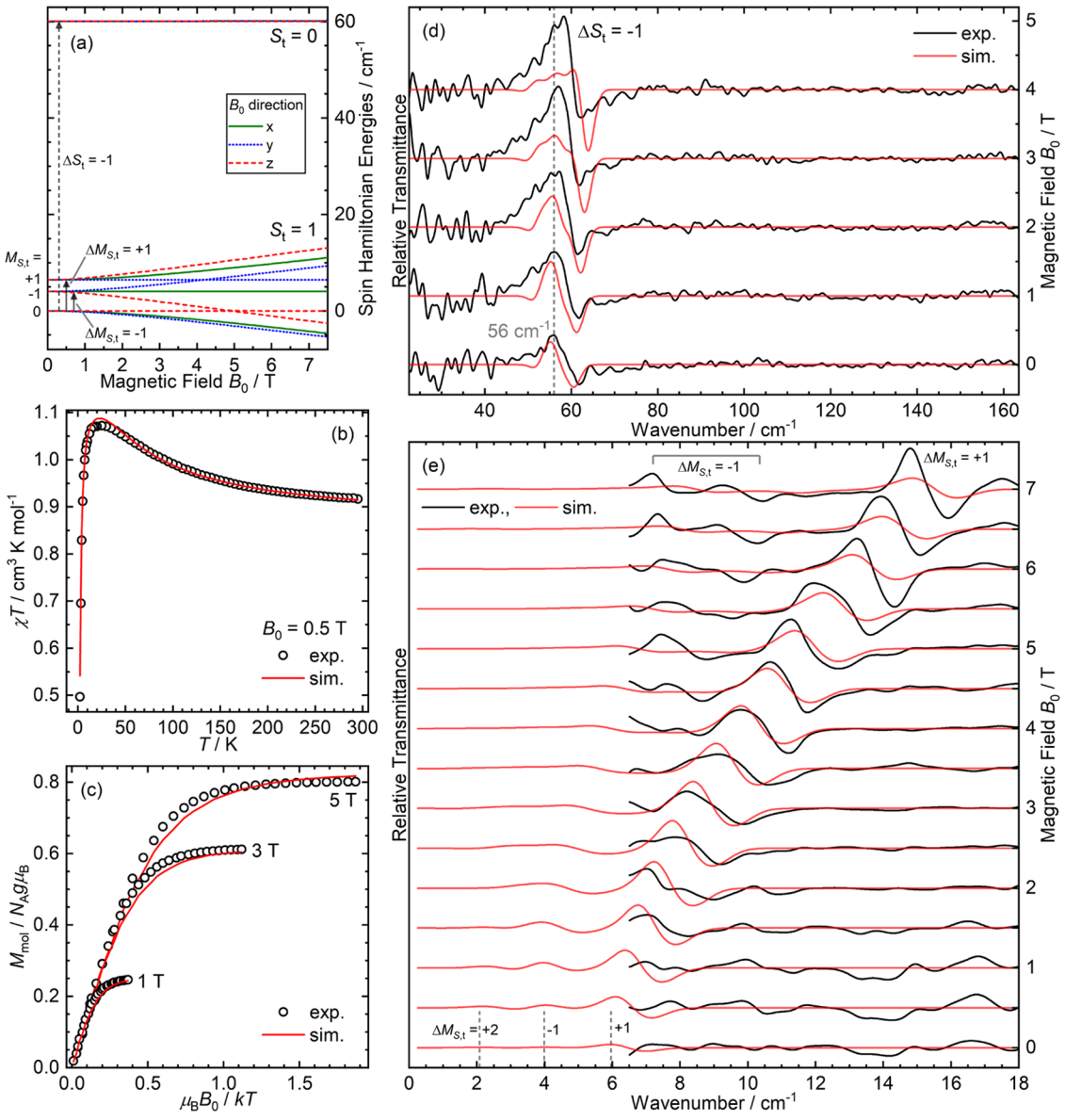

Figure 7. (a) Simulated field-dependent spin energy levels for **2** with B_0 aligned along the x, y, and z components of the ***d*** vector. Solid and dashed arrows indicate $\Delta M_{S,t}$ and ΔS_t transitions, respectively. (b, c) SQUID data points and simulated curves for crystalline samples of **2**: (b) χT vs T recorded at B_0 = 0.5 T and (c) iso-field magnetization M_{mol} recorded at 1, 3, and 5 T vs $\mu_B B_0/kT$. (d, e) FD-FT THz-EPR magnetic-field division spectra for pellets of polycrystalline **2** recorded at T = 5 K acquired using (d) low-α mode synchrotron radiation and (e) an Hg arc lamp. Spectra were calculated by division of a transmission spectrum recorded at (d) B_0 + 3 T or (e) B_0 + 0.5 T by a corresponding one measured at B_0 (see SI, Section 1.3). Thus, maxima correspond to stronger absorption at B_0 and minima to increased absorption at the higher field. Branches of $\Delta M_{S,t}$ = −1, $\Delta M_{S,t}$ = +1, and ΔS_t = −1 transitions are indicated, as well as $\Delta M_{S,t}$ = +2, −1, and +1 peak positions in the 0.5/0 T simulations in panel (e). Simulations in all panels are based on the optimized spin-Hamiltonian parameters in Table 2.

microscopic determination of spin coupling parameters, in particular in the presence of anisotropic exchange contributions, requires complementary spectroscopic information.[26−29] To fully assign the spin-Hamiltonian parameters in eq 1, accurately quantify the ZFS, and further elucidate its origin, SQUID magnetometry was complemented by FD-FT THz-EPR spectroscopy on complexes **2** and **B**.

Figure 7a depicts the calculated field-dependent spin energy level diagram for two coupled S_i = 1/2 centers with pronounced DM exchange (based on the parameters for **2**, Table 2). FD-FT THz-EPR determines the energies of allowed spin transitions between the $M_{S,t}$ = 0, ±1 levels within the S_t = 1 ground state, shown by solid arrows in Figure 7a. In addition, as will be demonstrated here for the first time, it can detect formally forbidden ΔS_t transitions between the ground state and the S_t = 0 excited state (dashed arrow) for coupled spins exhibiting antisymmetric exchange. Thereby, FD-FT THz-EPR at varying external magnetic fields allows for the independent extraction of g values and exchange coupling parameters according to eq 1, required for robust magnetostructural correlations. Figures 7d (S13d) and 7e (S13e) depict FD-FT THz-EPR spectra of complex **2** (**B**) in different experimentally accessible energy ranges, comprising the ΔS_t and $\Delta M_{S,t}$ transitions, respectively.

Zero-field FD-FT THz-EPR spectra, in principle, directly yield the triplet ZFS. However, in the present case, the ZFS is slightly lower than the low-energy boundary of the detection window, and signals are only observed at magnetic fields above

https://doi.org/10.1021/jacsau.2c00139
JACS Au 2022, 2, 1134−1143

Table 2. Optimized Spin-Hamiltonian Parameters for Complexes 2 and B from Global Simulations of the FD-FT THz-EPR and Magnetometry Data Using Equation 1[a]

	2	B
$g_{1,\perp}$	2.18	2.06[b]
$g_{1,\parallel}$	2.09	2.16[b]
$g_{2,\perp}$	2.09	2.06[b]
$g_{2,\parallel}$	2.25	2.16[b]
J_{iso}/cm^{-1}	25.4	76.9
$J_{ani,x}/cm^{-1}$	−0.9	−0.1
$J_{ani,y}/cm^{-1}$	1.5	1.2
$J_{ani,z}/cm^{-1}$	−0.6	−1.1
d_z/cm^{-1}	30.9	34.7

[a]For the Euler angles describing the orientations of the g tensors relative to the $\boldsymbol{d}$ frame, see Figure S16. [b]$\boldsymbol{g}$ tensors $\boldsymbol{g}_1$ and $\boldsymbol{g}_2$ of Cu1 and Cu2, respectively, were constrained to be identical.

1 T. Extrapolation of the peak positions toward lower fields confirms the large ZFS energy (i.e. $|D_t|$) for the total spin $S_t = 1$ ground state of 5−6 cm^{-1} for **2** and 3−4 cm^{-1} for **B** (for the corresponding effective spin-Hamiltonian, see Section 3.6 of the SI). Both complexes exhibit two main branches $\Delta M_{S,t} = -1$ and $\Delta M_{S,t} = +1$ of field-dependent lines with differing effective Zeeman shifts (in the 7.5/7 T spectra found at ∼7−10 and ∼14−16 cm^{-1}, respectively), which can be attributed to the transitions from $M_{S,t} = 0$ to the −1 and +1 sublevels, respectively (see below). In contrast to $\Delta M_{S,t} = +1$, an additional splitting is visible for the $\Delta M_{S,t} = -1$ transitions.

Most notably, in spectra at higher excitation energies, we could detect magnetic transitions with zero-field peaks of 56 cm^{-1} for complex **2** (Figure 7d) and 157 cm^{-1} for complex **B** (Figure S13d). They originate from the formally forbidden $\Delta S_t = -1$ transitions, indicating particular mixing of the uncoupled $|M_{S,1},M_{S,2}\rangle$ states that can only be engendered by the DM interaction.

For an exact quantification of the spin coupling parameters, we performed global multispin-Hamiltonian simulations of the FD-FT THz-EPR and magnetometry data. In the absence of local ZFS, only anisotropy of the exchange interaction, symmetric and/or antisymmetric, can account for the magnetic anisotropy. Simulations neglecting either $\hat{H}_{ani}$ or $\hat{H}_{DM}$ confirm that only the DM interaction induces a kind of mixing of the uncoupled $|M_{S,1},M_{S,2}\rangle$ states (for details see Section 3.6 in the SI) that results in a finite transition probability for the $S_t = 1 \rightarrow 0$ resonance to be observed around 56 cm^{-1} (**2**) and 157 cm^{-1} (**B**). The DM interaction is identified also as the main contribution to the ZFS by the spectral simulations in the following.

Since symmetric anisotropic exchange contributions are comparatively weak relative to isotropic and antisymmetric ones (see above),[30−32] $\hat{H}_{ani}$ was not considered in initial least-square fits. The orientations of the $\boldsymbol{g}$ tensors, assumed to be axial to reduce the number of parameters, were defined by spatially fitting a square pyramid or, in the case of Cu1 in **2**, a trigonal bipyramid to the atomic coordinates of the first coordination spheres of the Cu centers. The unique, axial components $g_z = g_\parallel$ were hence aligned approximately along Cu1−O1 and Cu2−N8 in **2** and Cu1−N5 and Cu2−N8 in **B** (Figure S16). They represent the smallest component in a trigonal pyramidal environment (d_{z^2} ground state)[a] and the largest in a square pyramidal environment ($d_{x^2-y^2}$ ground state),[32−35] as also found for the isolated Cu^{II} ion in the μ-1,2-superoxo complex upon $1e^-$ oxidation of **B**.[36] The orientation of the DM pseudovector $\boldsymbol{d}$ was defined such that the molecular pseudo-C_2 (**2**) or C_2 (**B**) axis coincides with its d_y component (Figure S16). In C_2-symmetric complex **B**, according to Moriya's symmetry rules,[17,18,37] the $\boldsymbol{d}$ vector has to be perpendicular to the C_2 axis, i.e., $d_y = 0$. Considering the relative orientation of the Cu1 and Cu2 square pyramids, their equatorial ligand planes are near-parallel, but they are rotated around their g_z axes by ∼66° relative to each other. Such a rotation results in orbital mixing, as shown theoretically,[19,31] here of $d_{x^2-y^2}$ and d_{xy}, engendering DM exchange in the direction of the rotation axis. Thus, the unique, nonzero DM vector component d_z was aligned along the average orientation of the Cu1 and Cu2 g_z axes. Despite the symmetry breaking by the different ligand side arms in complex **2**, a similar relative rotation of the ligand spheres by ∼92° can be conceived. The relevant axes from which the d_z orientation is deduced are, however, g_x of Cu1 and g_z of Cu2.

Simulations based on these models (Figures S12 and S14 and Table S1) provide a fitted isotropic exchange coupling J_{iso} = 25.3 cm^{-1} and a DM component d_z = 34.5 cm^{-1} for **2**, and J_{iso} = 76.1 cm^{-1} and d_z = 45.7 cm^{-1} for **B**, thus refining the values obtained previously from magnetometry (J_{iso} = 72 cm^{-1}, d_z = 42 cm^{-1}).[16] The respective spin-state energy schemes (Figures S12a and S14a) show that the $M_{S,t} = 0$ triplet sublevel is lowest in energy, corresponding to a positive ZFS $D_t > 0$. Thus, the branches of intratriplet transitions with the smaller and larger Zeeman shifts can be assigned to the transitions from $M_{S,t} = 0$ to −1 ($\Delta M_{S,t} = -1$) and +1 ($\Delta M_{S,t} = +1$), respectively. It is however seen that the simulations are not able to reproduce the splitting observed within the $\Delta M_{S,t} = -1$ transitions for both **2** and **B**. In addition, for complex **2**, the comparatively small Zeeman shift of the $\Delta S_t = -1$ transition is overestimated. While accounting for these issues by $\boldsymbol{g}$ tensor rhombicity yields unphysical values for g_x and g_y, an improved agreement is achieved by including the $\hat{H}_{ani}$ term (Figures 7 and S13 and Table 2), in particular reproducing the orientationally dependent $\Delta M_{S,t} = -1$ splitting (Figure S15; see also p. S15 of the SI for a discussion of the remaining discrepancies and limitations). At low fields, the simulations show peaks from the $\Delta M_{S,t} = +1$, $\Delta M_{S,t} = -1$, and $\Delta M_{S,t} = +2$ ($M_{S,t} = -1$ to +1) transitions at 6, 4, and 2.1 cm^{-1}, respectively, in **2** (3.8, 2.8, and 1 cm^{-1} for **B**). The symmetric anisotropic exchange is of reasonable size for this second-order SOC effect,[30−32] the unique component $J_{ani,y}$ = 1.5 cm^{-1} (**2**) and 1.2 cm^{-1} (**B**) of the traceless tensor being between one and two orders of magnitude smaller than J_{iso} and d_z, yet significantly larger than the calculated dipolar interaction (∼0.05 cm^{-1}). Its considerable contribution to the triplet-state ZFS engenders a reduction of d_z by 10% (**2**) and 24% (**B**) compared to the simulations neglecting $\hat{H}_{ani}$. In conclusion, the $\Delta M_{S,t} = -1$ splitting, i.e. differing transition energies in the x and y directions, results from rhombicity (E_t) in the triplet total spin ground state introduced by the symmetric anisotropic exchange. (It is noted that, while in the presence of $\hat{H}_{ani}$, $M_{S,t} = -1$ and +1 are no good quantum numbers, they are still being used analogous to the model without $\hat{H}_{ani}$; see SI, Section 3.6.)

The isolation and magnetic investigation of **2** allows for direct comparison of its magnetic properties with those of congeners **A** and **B**, revealing a linear correlation between the dihedral angle φ and the spin-spin coupling constant J_{iso} for these three systems (Figure 8a). Interestingly, even though

https://doi.org/10.1021/jacsau.2c00139
JACS Au 2022, 2, 1134−1143

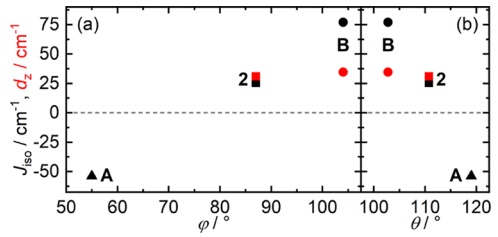

Figure 8. Correlation of the coupling constants J_{iso} (black) and d_z (red) with (a) Cu−O−O−Cu torsion angle φ and (b) Cu−O−O angle θ (average for both Cu ions) of complexes **2** (squares, Table 2), **B** (circles, Table 2), and **A**[16] (triangles).

complex **2** features a Cu−O−O−Cu torsion angle of nearly 90°, the extent of ferromagnetic coupling is significantly smaller than for the previously reported peroxodicopper(II) complex **B**, which exhibits a dihedral angle of 104°.[16] In theory,[38−40] the ferromagnetic coupling term should dominate when the magnetic orbitals approach orthogonality (φ = 90°), in which case the overlap integral of the magnetic orbitals is close to zero. However, this correlation has been derived for monoatomic bridges. It is not necessarily valid for extended bridges constituted by more than one atom over which the overlap density is spread, as already pointed out by Kahn.[38] DFT calculations show the delocalization of the magnetic orbitals (Section 4 in the SI) and yield an overlap integral of $S_{Overlap}$ = 0.09 for **2**, clearly larger than for complex **B** ($S_{Overlap}$ = 0.003). This is in accordance with the diminished ferromagnetic coupling in **2** despite a Cu−O−O−Cu torsion angle closer to 90°. If instead, the Cu−O−O angle θ is considered, in analogy to the pivotal angle for a monoatomic bridge, a much stronger angular dependence of J_{iso} is found (Figure 8b). From orbital considerations, it is highly plausible that a larger deviation of θ from orthogonality increases the overlap integral, providing an antiferromagnetic superexchange pathway. Thus, the concomitant increase of φ and decrease of θ shift the maximum ferromagnetic coupling to φ > 90° for μ-η^1:η^1-peroxodicopper(II) complexes. It can be presumed that in complexes with angles θ smaller than in **B**, J_{iso} will be even more ferromagnetic.

Correlating the magnitude of $\boldsymbol{d}$ (d_z) with φ and θ indicates different dependencies than for J_{iso}, with J_{iso} appearing to be more sensitive to the angular variations (Figure 8), as reported before.[41] In particular, the fact that significant DM exchange is still expected at the suggested zero-crossing points of J_{iso} renders the relation $|\boldsymbol{d}| \approx (\Delta g/g)|J_{iso}|$, derived by Moriya,[18] not entirely valid in this case. J_{iso} and d_z appear to be not directly proportional upon varying the binding motif, in accordance with distinctly different physical mechanisms representing dominant contributions to these and also the $\hat{H}_{ani}$ term.[31,41] As we have shown here, we can now separate and quantify these terms in a much more direct, accurate way using our approach. It will thus serve to gain deeper insight into how structural factors govern the various exchange contributions by applying it to further dicopper(II) complexes. It is noted that detection of ΔS_t = +1 (singlet-to-triplet) transitions should also allow us to characterize DM exchange in case of antiferromagnetic coupling. Furthermore, to determine the direction of the DM vectors $\boldsymbol{d}$ (and $\boldsymbol{J}_{ani}$) and their deviation from the z-axis, particularly for the asymmetrically distorted complex **2**, single-crystal experiments will be the method of choice.

CONCLUSIONS

Sophisticated ligand design has allowed to synthesize, in a targeted approach, a μ-η^1:η^1-peroxodicopper(II) complex (**2**) of the $^{\perp}$**P** type with a Cu−O−O−Cu torsion angle φ very close to 90°, emulating the arrangement and electronic situation that has been computationally proposed for the initial stages of O_2 binding at biological type III dicopper sites.[13−15] The isolation of **2** now provides a unique series of closely related and structurally characterized Cu_2/O_2 intermediates featuring μ-η^1:η^1-peroxodicopper(II) cores with φ values ranging from 55° (**A**, ^{C}**P** type)[11] via 87° (**2**, $^{\perp}$**P** type) up to 104° (**B**, in between $^{\perp}$**P** and ^{T}**P** type),[16] which allows us to experimentally establish a magnetostructural correlation for these biorelevant species. Because of the near-orthogonal Cu−O−O−Cu arrangement, magnetic coupling of the Cu^{II} ions in **2** is ferromagnetic, though slightly weaker than in **B**.

Correlations between spin state and reactivity have been extensively studied for biorelevant mononuclear iron-oxo, iron-superoxo, and iron-peroxo intermediates,[42,43] including the spin-state effect on the O−O bond rupture in the latter,[44,45] and spin topology contributions have also been discussed for the O−O bond cleavage in heme-peroxo-copper models of the cytochrome c oxidase active site.[46,47] Spin crossover processes accompanying such oxygen activation reactions, often proceeding via two-state reactivity, are known to be mediated by the SOC of the reactive transition metal ion. For single paramagnetic sites, the probability of a spin flip to occur depends on the mixing of the two spin states, for which the principal mechanism is the SOC interaction between the orbitals that become (de-)populated.[48] For triplet-to-singlet intersystem crossing during oxygen activation at type III copper sites (which does not involve an on-site electron transition), mixing of the spin states in the intermediate in which the spin crossover occurs will facilitate this process in an analogous manner. As the initial Cu_2/O_2 complex immediately after binding of triplet dioxygen to the dicopper(I) site is constrained to the triplet ground state, an efficient mixing mechanism appears to be essential. Antisymmetric exchange, originating from SOC and analyzed here in detail for two Cu_2/O_2 intermediate models, could be of utmost relevance in this respect. Thus, the present work now sets the scene for probing the spin state as a potential factor for the reactivity of bioinspired peroxodicopper(II) systems.

It is noted that the presented set of experimental data is the most comprehensive for coupled dicopper(II) complexes to date, including direct detection of the entirety of the spin-state transitions in the system. In particular, the observation of the formally forbidden ΔS_t = −1 transition is a novelty for coupled S = 1/2 spins without single-ion ZFS, providing unprecedented experimental insights into the DM exchange mechanism. Developments in the theoretical treatment of the DM interaction until now have been lacking experimentally determined values to benchmark the theories against.[19,31] Thus, this study paves the way for systematic investigations of compounds with varying binding geometries, which allow to scrutinize and refine theoretical models and will advance our understanding of DM exchange. Moreover, our methodology of FD-FT THz-EPR in combination with magnetometry can be extended to study DM interactions in Cu^{II} trimeric systems relevant for biological O_2 activation,[49,50] as well as molecular magnetism,[51] and further classes of materials (e.g. multiferroics[52,53]) where DM exchange is ascribed a decisive role for

https://doi.org/10.1021/jacsau.2c00139
JACS Au 2022, 2, 1134−1143

desired properties, such as spin-chiral magnetism[54] and magnetoelectric coupling.[55,56]

■ ASSOCIATED CONTENT

Supporting Information

The Supporting Information is available free of charge at https://pubs.acs.org/doi/10.1021/jacsau.2c00139.

Experimental as well as synthetic procedures and further spectroscopic and analytical data, crystallographic information, and details of the DFT calculations (PDF)

Accession Codes

CCDC 2155127−2155128 contain the supplementary crystallographic data for this paper. These data can be obtained free of charge via www.ccdc.cam.ac.uk/data_request/cif, or by emailing data_request@ccdc.cam.ac.uk, or by contacting The Cambridge Crystallographic Data Centre, 12 Union Road, Cambridge CB2 1EZ, UK; fax: +44 1223 336033.

■ AUTHOR INFORMATION

Corresponding Authors

Alexander Schnegg − *Max Planck Institute for Chemical Energy Conversion, D-45470 Mülheim an der Ruhr, Germany;* orcid.org/0000-0002-2362-0638; Email: alexander.schnegg@cec.mpg.de

Franc Meyer − *University of Göttingen, Institute of Inorganic Chemistry, D-37077 Göttingen, Germany; University of Göttingen, International Center for Advanced Studies of Energy Conversion (ICASEC), D-37077 Göttingen, Germany;* orcid.org/0000-0002-8613-7862; Email: franc.meyer@chemie.uni-goettingen.de

Authors

Thomas Lohmiller − *EPR4Energy Joint Lab, Department Spins in Energy Conversion and Quantum Information Science, Helmholtz Zentrum Berlin für Materialien und Energie GmbH, 12489 Berlin, Germany;* Present Address: Humboldt-Universität zu Berlin, Institut für Chemie, Brook-Taylor-Str. 2, 12489 Berlin, Germany; orcid.org/0000-0003-0373-1506

Can-Jerome Spyra − *University of Göttingen, Institute of Inorganic Chemistry, D-37077 Göttingen, Germany*

Sebastian Dechert − *University of Göttingen, Institute of Inorganic Chemistry, D-37077 Göttingen, Germany;* orcid.org/0000-0002-2864-2449

Serhiy Demeshko − *University of Göttingen, Institute of Inorganic Chemistry, D-37077 Göttingen, Germany*

Eckhard Bill − *Max Planck Institute for Chemical Energy Conversion, D-45470 Mülheim an der Ruhr, Germany;* orcid.org/0000-0001-9138-3964

Complete contact information is available at: https://pubs.acs.org/10.1021/jacsau.2c00139

Author Contributions

#T.L. and C.-J.S. contributed equally to this work.

Funding

This work was supported by the University of Göttingen and by the Max Planck Society (MPI CEC).

Notes

The authors declare no competing financial interest.

■ ACKNOWLEDGMENTS

The authors thank Helmholtz-Zentrum Berlin for the allocation of synchrotron radiation beamtime at BESSY II (201-09196). The authors are grateful to Dr. Joscha Nehrkorn, Dr. Karsten Holldack, and Dirk Ponwitz for assistance with the FD-FT THz-EPR experiments.

■ ADDITIONAL NOTE

[a]Symbols for d orbitals and the d_i (i = x, y, z) components of the DM vector are written in normal and italic fonts, respectively.

■ REFERENCES

(1) Solomon, E. I.; Sundaram, U. M.; Machonkin, T. E. Multicopper Oxidases and Oxygenases. *Chem. Rev.* **1996**, *96*, 2563−2605.

(2) Lewis, E. A.; Tolman, W. B. Reactivity of Dioxygen − Copper Systems. *Chem. Rev.* **2004**, *104*, 1047−1076.

(3) Solomon, E. I.; Heppner, D. E.; Johnston, E. M.; Ginsbach, J. W.; Cirera, J.; Qayyum, M.; Kieber-Emmons, M. T.; Kjaergaard, C. H.; Hadt, R. G.; Tian, L. Copper Active Sites in Biology. *Chem. Rev.* **2014**, *114*, 3659−3853.

(4) Mirica, L. M.; Ottenwaelder, X.; Stack, T. D. P. Structure and Spectroscopy of Copper-Dioxygen Complexes. *Chem. Rev.* **2004**, *104*, 1013−1045.

(5) Solomon, E. I.; Ginsbach, J. W.; Heppner, D. E.; Kieber-Emmons, M. T.; Kjaergaard, C. H.; Smeets, P. J.; Tian, L.; Woertink, J. S. Copper Dioxygen (Bio)Inorganic Chemistry. *Faraday Discuss.* **2011**, *148*, 11−39.

(6) Elwell, C. E.; Gagnon, N. L.; Neisen, B. D.; Dhar, D.; Spaeth, A. D.; Yee, G. M.; Tolman, W. B. Copper-Oxygen Complexes Revisited: Structures, Spectroscopy, and Reactivity. *Chem. Rev.* **2017**, *117*, 2059−2107.

(7) Jacobson, R. R.; Tyeklar, Z.; Farooq, A.; Karlin, K. D.; Liu, S.; Zubieta, J. A Cu_2-O_2 Complex. Crystal Structure and Characterization of a Reversible Dioxygen Binding System. *J. Am. Chem. Soc.* **1988**, *110*, 3690−3692.

(8) Kitajima, N.; Fujisawa, K.; Moro-oka, Y. M-η^2:η^2- Peroxo Binuclear Copper Complex, $[Cu(HB(2,5\text{-}IPr_2Pz)_3)]_2(O_2)$. *J. Am. Chem. Soc.* **1989**, *111*, 8975−8976.

(9) Halfen, J. A.; Mahapatra, S.; Wilkinson, E. C.; Kaderli, S.; Young, V. G.; Que, L.; Zuberbühler, A. D.; Tolman, W. B. Reversible Cleavage and Formation of the Dioxygen O-O Bond within a Dicopper Complex. *Science* **1996**, *271*, 1397−1400.

(10) Dalle, K. E.; Gruene, T.; Dechert, S.; Demeshko, S.; Meyer, F. Weakly Coupled Biologically Relevant $Cu_2^{II}(\mu\text{-}\eta^1\text{:}\eta^1\text{-}O_2)$ Cis -Peroxo Adduct That Binds Side-on to Additional Metal Ions. *J. Am. Chem. Soc.* **2014**, *136*, 7428−7434.

(11) Brinkmeier, A.; Schulz, R. A.; Buchhorn, M.; Spyra, C. J.; Dechert, S.; Demeshko, S.; Krewald, V.; Meyer, F. Structurally Characterized μ-1,2-Peroxo/Superoxo Dicopper(II) Pair. *J. Am. Chem. Soc.* **2021**, *143*, 10361−10366.

(12) Brinkmeier, A.; Dalle, K. E.; D'Amore, L.; Schulz, R. A.; Dechert, S.; Demeshko, S.; Swart, M.; Meyer, F. Modulation of a μ-1,2-Peroxo Dicopper(II) Intermediate by Strong Interaction with Alkali Metal Ions. *J. Am. Chem. Soc.* **2021**, *143*, 17751−17760.

(13) Metz, M.; Solomon, E. I. Dioxygen Binding to Deoxyhemocyanin: Electronic Structure and Mechanism of the Spin-Forbidden Two-Electron Reduction of O_2. *J. Am. Chem. Soc.* **2001**, *123*, 4938−4950.

(14) Solomon, E. I.; Chen, P.; Metz, M.; Lee, S. K.; Palmer, A. E. Oxygen Binding, Activation, and Reduction to Water by Copper Proteins. *Angew. Chem., Int. Ed.* **2001**, *40*, 4570−4590.

(15) Solomon, E. I. Dioxygen Binding, Activation, and Reduction to H_2O by Cu Enzymes. *Inorg. Chem.* **2016**, *55*, 6364−6375.

(16) Kindermann, N.; Bill, E.; Dechert, S.; Demeshko, S.; Reijerse, E. J.; Meyer, F. A Ferromagnetically Coupled (S = 1) Peroxodicopper-(II) Complex. *Angew. Chem., Int. Ed.* **2015**, *54*, 1738−1743.

(17) Moriya, T. New Mechanism of Anisotropic Superexchange Interaction. *Phys. Rev. Lett.* **1960**, *4*, 228−230.
(18) Moriya, T. Anisotropic Superexchange Interaction and Weak Ferromagnetism. *Phys. Rev.* **1960**, *120*, 91−98.
(19) Bouammali, M.-A.; Suaud, N.; Martins, C.; Maurice, R.; Guihéry, N. How to Create Giant Dzyaloshinskii−Moriya Interactions? Analytical Derivation and Ab Initio Calculations on Model Dicopper(II) Complexes. *J. Chem. Phys.* **2021**, *154*, No. 134301.
(20) Nehrkorn, J.; Telser, J.; Holldack, K.; Stoll, S.; Schnegg, A. Simulating Frequency-Domain Electron Paramagnetic Resonance: Bridging the Gap between Experiment and Magnetic Parameters for High-Spin Transition-Metal Ion Complexes. *J. Phys. Chem. B* **2015**, *119*, 13816−13824.
(21) Nehrkorn, J.; Holldack, K.; Bittl, R.; Schnegg, A. Recent Progress in Synchrotron-Based Frequency-Domain Fourier-Transform THz-EPR. *J. Magn. Reson.* **2017**, *280*, 10−19.
(22) Buchler, S.; Meyer, F.; Kaifer, E.; Pritzkow, H. Tunable TACN/Pyrazolate Hybrid Ligands as Dinucleating Scaffolds for Metallobiosite Modeling - Dinickel(II) Complexes Relevant to the Urease Active Site. *Inorg. Chim. Acta* **2002**, *337*, 371−386.
(23) Dalle, K. E.; Dechert, S.; Meyer, F. Improved Synthesis and Detailed Characterization of a Hybrid Pyrazole-TACN Dinucleating Ligand. *Z. Anorg. Allg. Chem.* **2015**, *641*, 2181−2189.
(24) Yang, L.; Powell, D. R.; Houser, R. P. Structural Variation in Copper(I) Complexes with Pyridylmethylamide Ligands: Structural Analysis with a New Four-Coordinate Geometry Index, τ_4. *Dalton Trans.* **2007**, *9*, 955−964.
(25) Karlin, K. D.; Tyeklár, Z.; Farooq, A.; Jacobson, R. R.; Sinn, E.; Lee, D. W.; Bradshaw, J. E.; Wilson, L. J. Peroxide (O_2^{2-}) as a Bridging Ligand for Copper(II): Strong Exchange Coupling in Complexes Derived from Copper(I) and Dioxygen. *Inorg. Chim. Acta* **1991**, *182*, 1−3.
(26) Pedersen, K. S.; Dreiser, J.; Nehrkorn, J.; Gysler, M.; Schau-Magnussen, M.; Schnegg, A.; Holldack, K.; Bittl, R.; Piligkos, S.; Weihe, H.; Tregenna-Piggott, P.; Waldmann, O.; Bendix, J. A Linear Single-Molecule Magnet Based on $[Ru^{III}(CN)_6]^{3-}$. *Chem. Commun.* **2011**, *47*, 6918−6920.
(27) Dreiser, J.; Pedersen, K. S.; Schnegg, A.; Holldack, K.; Nehrkorn, J.; Sigrist, M.; Tregenna-Piggott, P.; Mutka, H.; Weihe, H.; Mironov, V. S.; Bendix, J.; Waldmann, O. Three-Axis Anisotropic Exchange Coupling in the Single-Molecule Magnets $NEt_4[Mn^{III}2(5\text{-}Brsalen)_2(MeOH)_2M^{III}(CN)_6]$ (M=Ru, Os). *Chem. - Eur. J.* **2013**, *19*, 3693−3701.
(28) Pinkowicz, D.; Southerland, H. I.; Avendaño, C.; Prosvirin, A.; Sanders, C.; Wernsdorfer, W.; Pedersen, K. S.; Dreiser, J.; Clérac, R.; Nehrkorn, J.; Simeoni, G. G.; Schnegg, A.; Holldack, K.; Dunbar, K. R. Cyanide Single-Molecule Magnets Exhibiting Solvent Dependent Reversible "On" and "Off" Exchange Bias Behavior. *J. Am. Chem. Soc.* **2015**, *137*, 14406−14422.
(29) Rams, M.; Jochim, A.; Böhme, M.; Lohmiller, T.; Ceglarska, M.; Rams, M. M.; Schnegg, A.; Plass, W.; Näther, C. Single-Chain Magnet Based on Cobalt(II) Thiocyanate as XXZ Spin Chain. *Chem. - Eur. J.* **2020**, *26*, 2837−2851.
(30) McGregor, K. T.; Soos, Z. G. Anisotropic Exchange in Linear Chain Complexes of Copper(II). *J. Chem. Phys.* **1976**, *64*, 2506.
(31) Maurice, R.; Pradipto, A. M.; Guihéry, N.; Broer, R.; de Graaf, C. Antisymmetric Magnetic Interactions in Oxo-Bridged Copper(II) Bimetallic Systems. *J. Chem. Theory Comput.* **2010**, *6*, 3092−3101.
(32) Atanasov, M.; Comba, P.; Hanson, G. R.; Hausberg, S.; Helmle, S.; Wadepohl, H. Cyano-Bridged Homodinuclear Copper(II) Complexes. *Inorg. Chem.* **2011**, *50*, 6890−6901.
(33) Barbucci, R.; Campbell, M. J. M. EPR Spectra of Trigonal Bipyramidal Copper(II) Species $Cu(R_6tren)X^+$. *Inorg. Chim. Acta* **1975**, *15*, L15−L16.
(34) Hathaway, B. J.; Billing, D. E. The Electronic Properties and Stereochemistry of Mono-Nuclear Complexes of the Copper(II) Ion. *Coord. Chem. Rev.* **1970**, *5*, 143−207.
(35) Tamayo, A.; Casabó, J.; Escriche, L.; González, P.; Lodeiro, C.; Rizzi, A. C.; Brondino, C. D.; Passeggi, M. C. G.; Kivekäs, R.; Sillanpää, R. Structural and EPR Studies on Single-Crystal and Polycrystalline Samples of Copper(II) and Cobalt(II) Complexes with N2S2-Based Macrocyclic Ligands. *Inorg. Chem.* **2007**, *46*, 5665−5672.
(36) Kindermann, N.; Günes, C.-J.; Dechert, S.; Meyer, F. Hydrogen Atom Abstraction Thermodynamics of a μ-1,2-Superoxo Dicopper(II) Complex. *J. Am. Chem. Soc.* **2017**, *139*, 9831−9834.
(37) Buckingham, A. D.; Pyykkö, P.; Robert, J. B.; Wiesenfeld, L. Symmetry Rules for the Indirect Nuclear Spin-Spin Coupling Tensor Revisited. *Mol. Phys.* **1982**, *46*, 177−182.
(38) Kahn, O. Dinuclear Complexes with Predictable Magnetic Properties. *Angew. Chem., Int. Ed.* **1985**, *24*, 834−850.
(39) Girerd, J. J.; Charlot, M. F.; Kahn, O. Orbital Interaction in One-Dimensional Magnetic Compounds. *Mol. Phys.* **1977**, *34*, 1063−1076.
(40) Girerd, J. J.; Journaux, Y.; Kahn, O. Natural or Orthogonalized Magnetic Orbitals: Two Alternative Ways to Describe the Exchange Interaction. *Chem. Phys. Lett.* **1981**, *82*, 534−538.
(41) Charlot, M. F.; Journaux, Y.; Kahn, O.; Bencini, A.; Gatteschi, D.; Zanchini, C. Anisotropic Exchange in Bibridged Copper(II) Dimers: A Topological Approach. *Inorg. Chem.* **1986**, *25*, 1060−1063.
(42) Usharani, D.; Janardanan, D.; Li, C.; Shaik, S. A Theory for Bioinorganic Chemical Reactivity of Oxometal Complexes and Analogous Oxidants: The Exchange and Orbital-Selection Rules. *Acc. Chem. Res.* **2013**, *46*, 471−482.
(43) Ye, S.; Geng, C.-Y.; Shaik, S.; Neese, F. Electronic Structure Analysis of Multistate Reactivity in Transition Metal Catalyzed Reactions: The Case of C−H Bond Activation by Non-Heme Iron(IV)−Oxo Cores. *Phys. Chem. Chem. Phys.* **2013**, *15*, 8017−8030.
(44) Liu, L. V.; Hong, S.; Cho, J.; Nam, W.; Solomon, E. I. Comparison of High-Spin and Low-Spin Nonheme FeIII−OOH Complexes in O−O Bond Homolysis and H-Atom Abstraction Reactivities. *J. Am. Chem. Soc.* **2013**, *135*, 3286−3299.
(45) Jeon, H.; Hong, S. Peroxide Bond Cleavage of Nonheme Iron-(Hydro/Alkyl)Peroxo Complexes Induced by Endogenous and Exogenous Factors. *Chem. Lett.* **2019**, *48*, 80−85.
(46) Kieber-Emmons, M. T.; Li, Y.; Halime, Z.; Karlin, K. D.; Solomon, E. I. Electronic Structure of a Low-Spin Heme/Cu Peroxide Complex: Spin-State and Spin-Topology Contributions to Reactivity. *Inorg. Chem.* **2011**, *50*, 11777−11786.
(47) Schaefer, A. W.; Roveda, A. C.; Jose, A.; Solomon, E. I. Geometric and Electronic Structure Contributions to O−O Cleavage and the Resultant Intermediate Generated in Heme-Copper Oxidases. *J. Am. Chem. Soc.* **2019**, *141*, 10068−10081.
(48) Danovich, D.; Shaik, S. Spin−Orbit Coupling in the Oxidative Activation of H−H by FeO^+. Selection Rules and Reactivity Effects. *J. Am. Chem. Soc.* **1997**, *119*, 1773−1786.
(49) Yoon, J.; Mirica, L. M.; Stack, T. D. P.; Solomon, E. I. Spectroscopic Demonstration of a Large Antisymmetric Exchange Contribution to the Spin-Frustrated Ground State of AD3Symmetric Hydroxy-Bridged Trinuclear Cu(II) Complex: Ground-to-Excited State Superexchange Pathways. *J. Am. Chem. Soc.* **2004**, *126*, 12586−12595.
(50) Yoon, J.; Solomon, E. I. Electronic Structures of Exchange Coupled Trigonal Trimeric Cu(II) Complexes: Spin Frustration, Antisymmetric Exchange, Pseudo-A Terms, and Their Relation to O2 Activation in the Multicopper Oxidases. *Coord. Chem. Rev.* **2007**, *251*, 379−400.
(51) Boudalis, A. K. Half-Integer Spin Triangles: Old Dogs, New Tricks. *Chem. - Eur. J.* **2021**, *27*, 7022−7042.
(52) Sergienko, I. A.; Dagotto, E. Role of the Dzyaloshinskii-Moriya Interaction in Multiferroic Perovskites. *Phys. Rev. B* **2006**, *73*, No. 094434.
(53) Lottermoser, T.; Meier, D. A Short History of Multiferroics. *Phys. Sci. Rev.* **2021**, *6*, 1−11.
(54) Mandru, A.-O.; Yıldırım, O.; Tomasello, R.; Heistracher, P.; Penedo, M.; Giordano, A.; Suess, D.; Finocchio, G.; Hug, H. J. Coexistence of Distinct Skyrmion Phases Observed in Hybrid

https://doi.org/10.1021/jacsau.2c00139
JACS Au 2022, 2, 1134−1143

Ferromagnetic/Ferrimagnetic Multilayers. *Nat. Commun.* **2020**, *11*, No. 6365.
(55) Stepanenko, D.; Trif, M.; Tsyplyatyev, O.; Loss, D. Field-Dependent Superradiant Quantum Phase Transition of Molecular Magnets in Microwave Cavities. *Semicond. Sci. Technol.* **2016**, *31*, No. 094003.
(56) Robert, J.; Parizel, N.; Turek, P.; Boudalis, A. K. Polyanisotropic Magnetoelectric Coupling in an Electrically Controlled Molecular Spin Qubit. *J. Am. Chem. Soc.* **2019**, *141*, 19765−19775.

https://doi.org/10.1021/jacsau.2c00139
JACS Au 2022, 2, 1134−1143